

Lu Cao · You-Chang Yang · Hong Chen

Charmonium states in QCD-inspired quark potential model using Gaussian expansion method

Received: date / Accepted: date

Abstract We study the mass spectrum and electromagnetic processes of charmonium system with the spin-dependent potentials fully taking into account in the solution of the Schroedinger equation and the results for the pure scalar and scalar-vector mixing linear confining potentials are compared. It is revealed that the scalar-vector mixing confinement is important for reproducing the mass spectrum and decay widths and the vector component is found to be around 22%, the long-standing discrepancy in M1 radiative transitions of J/ψ and ψ' is alleviated by means of the state wave functions obtained via the Hamiltonian with the full spin-dependent potential. This work also intends to identify few of the copious higher charmonium-like states as the $c\bar{c}$ ones. Particularly, the newly observed $X(4160)$ and $X(4350)$ are assigned as $M(2^1D_2) = 4164.9$ MeV and $M(3^3P_2) = 4352.4$ MeV, which strongly favor the $J^{PC} = 2^{-+}, 2^{++}$ assignments respectively. The corresponding radiative transitions, leptonic and two-photon decay widths have been also calculated for the further experimental study.

Keywords charmonium · potential model · Gaussian expansion method · XYZ mesons

1 Introduction

Due to the impressive increase of experimental results, charmonium ($c\bar{c}$) spectroscopy has renewed great interest recently, coming along with the striking disagreement with theoretical expectations [1, 2, 3]. The unexpected and still-fascinating $X(3872)$ has been joined by more than a dozen other charmonium-like states, while the series of vacancy have been left on the $c\bar{c}$ list. It is urgent to identify the possible new members of charmonium family from the abundant observations.

The QCD inspired potential models have been playing an important role in investigating heavy quarkonium, owing to the presence of large nonperturbative effects in this energy region. Most quark potential models [4, 5, 6, 7, 8, 9, 10, 11, 12, 13, 14, 15, 16] have common ingredients under the non-relativistic limit, despite some differences in the detailed corrections for relativistic and coupled channel effects, which typically are the Coulomb-like term induced by one-gluon exchange plus the long-range confining potential expected from nonperturbative QCD. Anyway, the nature of confining mechanism has been veiled so far. In the original Cornell model [17, 18], it was assumed as Lorentz scalar, which gives a vanishing long-range magnetic contribution and agrees with the flux tube picture of quark

Lu Cao
School of Physical Science and Technology, Southwest University, Chongqing 400700, China
E-mail: physicaolu@126.com

You-Chang Yang
Department of Physics, Zunyi Normal College, Zunyi 563002, China
E-mail: yangyouchang@yahoo.com.cn

Hong Chen
School of Physical Science and Technology, Southwest University, Chongqing 400700, China
Corresponding Author. E-mail: chenh@swu.edu.cn

confinement [19]. Another possibility [9, 20] is that confinement may be a more complicated mixture of scalar and timelike vector, while the vector potential is anticonfining. In pure $c\bar{c}$ models, the Lorentz nature of confinement is tested by the multiplet splitting of orbitally excited charmonium states.

In addition, numerical precision of the calculation method is important in testing different models. As several numerical methods fail in the potentials with $1/r^2$ and even higher negative power, the $\mathcal{O}(v^2/c^2)$ corrections to the quark-antiquark potential has to be usually treated as perturbation [21, 22, 20]. However, the accuracy of perturbation expansion has been alerted recently [23], which indicates the most significant effect of the different treatments is on the wave functions. The exact solution of the full Hamiltonian provides every state with its own wave function, while the perturbative treatment leads to the same angular momentum multiplets sharing the identical radial wave function. It is known that the radiative transitions, leptonic and double-photon decay widths are quite sensitive to the shape of wave function and its behavior at the origin. Each physical particle with different quantum numbers should have different state wave function. Thus, it is interesting to study the still-puzzling confining mechanism and the numerical precision of the calculation method.

In our calculation framework, the spin-dependent and -independent interactions have been totally taken into account in the Hamiltonian, where the different confining assumptions are compared from the mass spectrum and decay properties. The precise wave functions are inspected through the electromagnetic processes, i.e. radiative transitions and leptonic decays, which are considered to be a nichetargeting test for the overlap of radial integration and the subtle information at the origin. Since the relativistic reconstruction of the static confining potential is not unique, it complicates the nature of confinement. Hence special concerns are focused on the minimal but relatively well-understood models, with the aim of gleaning the actual influences of different forms of confinement potential and the difference between the exact and the perturbative solutions.

In the following section, the two potential models are described in detail, along with the adopted variational approach and the optimization of parameters. The numerical results are assembled in Sec.3, a discussion related to the latest experimental results are put in Sec.4. Finally, Sec.5 summaries the remarks and conclusions.

2 Potential models and calculational approach

The confinement of quarks is assumed to be purely scalar linear type in NR model[21], and the scalar-vector mixed one in MNR [9]. Once the Lorentz structure of central part are fixed in the two forms,

$$\text{NR: } V_S = b r; \quad V_V = -\frac{4}{3} \frac{\alpha_s}{r}, \quad (1)$$

$$\text{MNR: } V_S = b(1 - \epsilon)r; \quad V_V = -\frac{4}{3} \frac{\alpha_s}{r} + \epsilon b r, \quad (2)$$

the spin-orbit term and the tensor term can be directly derived from the standard Breit-Fermi expression to order (v^2/c^2) with the charmed quark mass m_c . Summarily, the interaction potentials are

$$V_{NR} = -\frac{4}{3} \frac{\alpha_s}{r} + b r + \frac{32\pi\alpha_s}{9m_c^2} \tilde{\delta}_\sigma(r) \mathbf{S}_c \cdot \mathbf{S}_{\bar{c}} + \left[\frac{2\alpha_s}{m_c^2 r^3} - \frac{b}{2m_c^2 r} \right] \mathbf{L} \cdot \mathbf{S} + \frac{4\alpha_s}{m_c^2 r^3} \mathbf{T}, \quad (3)$$

$$V_{MNR} = -\frac{4}{3} \frac{\alpha_s}{r} + b r + \frac{32\pi\alpha_s}{9m_c^2} \tilde{\delta}_\sigma(r) \mathbf{S}_c \cdot \mathbf{S}_{\bar{c}} + \left[\frac{2\alpha_s}{m_c^2 r^3} + \frac{(4\epsilon - 1)b}{2m_c^2 r} \right] \mathbf{L} \cdot \mathbf{S} + \left[\frac{\alpha_s}{3m_c^2 r^3} + \frac{\epsilon b}{12m_c^2 r} \right] \mathbf{T}, \quad (4)$$

where \mathbf{L} is the orbital momentum and \mathbf{S} is the spin of charmonium. In the mixed-confining model, ϵ stands for the vector exchange scale. The singularity of contact hyperfine interaction within the spin-spin term has been smeared by Gaussian as in Ref.[21], $\tilde{\delta}_\sigma(r) = (\sigma/\sqrt{\pi})^3 e^{-\sigma^2 r^2}$. The involved operators are diagonal in a $|\mathbf{J}, \mathbf{L}, \mathbf{S}\rangle$ basis with the matrix elements,

$$\langle \mathbf{S}_c \cdot \mathbf{S}_{\bar{c}} \rangle = \frac{1}{2} S(S+1) - \frac{3}{4}, \quad (5)$$

$$\langle \mathbf{L} \cdot \mathbf{S} \rangle = \frac{1}{2} [J(J+1) - L(L+1) - S(S+1)], \quad (6)$$

Table 1 Basis-related parameters for the potential models

	Parameter	NR	MNR
Basis Space	n_{max}	10	8
	r_1 [GeV ⁻¹]	0.4	0.4
	$r_{n_{max}}$ [GeV ⁻¹]	15.8	6.8
Potential Model	m_c [GeV]	1.4786	1.5216
	α_s	0.5761	0.6344
	b [GeV ²]	0.1468	0.1361
	σ [GeV]	1.1384	1.2058
	ϵ	-	-0.2193

$$\langle \mathbf{T} \rangle = \left\langle \left[\frac{3}{r^2} (\mathbf{S}_c \cdot \mathbf{r})(\mathbf{S}_{\bar{c}} \cdot \mathbf{r}) - (\mathbf{S}_c \cdot \mathbf{S}_{\bar{c}}) \right] \right\rangle = -\frac{6(\langle \mathbf{L} \cdot \mathbf{S} \rangle)^2 + 3\langle \mathbf{L} \cdot \mathbf{S} \rangle - 2S(S+1)L(L+1)}{6(2L-1)(2L+3)}. \quad (7)$$

Instead of separating the spin-dependent interactions into leading order portions, we solved the Schroedinger equation of the unperturbed Hamiltonian with full potentials,

$$\left[-\frac{\hbar^2}{2\mu_R} \nabla^2 + V_{c\bar{c}}(r) - E \right] \psi(\mathbf{r}) = 0, \quad (8)$$

where $\mu_R = m_c/2$ is the reduced mass. Here, $V_{c\bar{c}}(r)$ is V_{NR} or V_{MNR} which includes the spin-independent interactions as well as the spin-dependent ones. The Hamiltonian includes the full potential, enable us to maintain the subtleness of wave function. With the help of a well-chosen set of Gaussian basis functions, namely Gaussian Expansion Method [24], the singular behavior of $1/r^3$ in spin-dependent terms at short distance can be refined variationally. Then, the wave functions $\psi_{lm}(\mathbf{r})$ are expanded in terms of a set of Gaussian basis functions as

$$\psi_{lm}(\mathbf{r}) = \sum_{n=1}^{n_{max}} C_{nl} \left(\frac{2^{2l+\frac{7}{2}} \nu_n^{l+\frac{3}{2}}}{\sqrt{\pi}(2l+1)!!} \right)^{\frac{1}{2}} r^l e^{-(r/r_n)^2} Y_{lm}(\hat{\mathbf{r}}), \quad (9)$$

$$\nu_n = \frac{1}{r_n^2}, \quad r_n = r_1 a^{n-1}. \quad (10)$$

The basis-related parameters $\{n_{max}, r_1, r_n\}$ are determined by the variational principle, resulting the reasonably stable eigen solutions and differ slightly according to the explicit forms of potential models. Table 1 shows the utilized basis for the two potential models.

To determine the parameters ($\mathbf{a} = a_1, a_2, \dots, a_P$) appearing in the potentials, a merit function χ^2 has been defined to search the best-fit parameters by its minimization,

$$\chi^2 = \sum_{i=1}^N \left[\frac{M_i^{exp} - M_i^{th}(\mathbf{a})}{\sigma_i} \right]^2, \quad (11)$$

where N denotes the number of targeted data, the σ are the associated errors and M_i represents the experimental and theoretical values. Given a trial set of model-depended parameters, a procedure calculating the $\chi^2(\mathbf{a})$ are developed to improve the trial solution with the increments $\delta \mathbf{a}$ and repeated until $\chi^2(\mathbf{a} + \delta \mathbf{a})$ effectively stops decreasing. The increments $\delta \mathbf{a}$ are solved by the set of linear equations

$$\sum_{j=1}^P \alpha_{kj} \delta a_j = \beta_k, \quad (12)$$

with

$$\beta_k \equiv -\frac{1}{2} \frac{\partial \chi^2}{\partial a_k} \quad (13)$$

$$\alpha_{kj} = \sum_{i=1}^N \frac{1}{\sigma_i^2} \left[\frac{\partial M_i^{th}(\mathbf{a})}{\partial a_k} \frac{\partial M_i^{th}(\mathbf{a})}{\partial a_j} \right]. \quad (14)$$

The iteration has been taken in the numerical analysis of nonlinear systems. Here, the partial derivative has to be solved numerically because the $M_i^{th}(\mathbf{a})$ is not analytic.

3 Numerical Results

3.1 Mass Spectrum

Combining the nonrelativistic kinetic term and the interactions terms, we diagonalize the full Hamiltonian, which leads to a generalized eigenvalue problem. After the fitting procedure, the energy levels and corresponding eign functions of the two potential models are obtained with its optimized parameter set (shown in Table 1).

The vector component of linear confining are fitted to be 21.93% for the MNR model. This result consists with the one-fifth vector exchange given by Ref. [23]. If defined an additional r -independent adjustable parameter in the vector linear confinement, the value of mixing coefficient should be -1 for some decay considerations [20]. In addition, the scalar-vector mixing model requires less linear potential slope, but more splitting scale from spin-spin interaction.

Totally 60 states have been calculated with the two potential models, and summarized in Table 2. We fit the mass of well-established states marked by *. Except somewhat low at $\chi_0(1^3P_0)$, both of the two potential models are overall good to reproduce the spectrum.

3.2 Leptonic Decays

The lowest-order expressions of electronic decay width the first-order QCD corrections [26] are

$$\Gamma_{ee}(nS) = \frac{4\alpha^2 e_c^2}{M_{nS}^2} |R_{nS}(0)|^2 \left(1 - \frac{16}{3} \frac{\alpha_s(m_c)}{\pi}\right), \quad (15)$$

$$\Gamma_{ee}(nD) = \frac{25\alpha^2 e_c^2}{2M_{nD}^2 M_Q^4} |R''_{nD}(0)|^2 \left(1 - \frac{16}{3} \frac{\alpha_s(m_c)}{\pi}\right), \quad (16)$$

where e_c is the c-quark charge in units of $|e|$, $\alpha = 1/137.036$ is the fine-structure constant, M_{nS} and M_{nD} are the $(n_r + 1)th$ S-wave and D-wave state mass respectively with the radial excitation number n_r . Note that here $\alpha_s(m_c)$ and the α_s are essentially the strong coupling constants of different mass scales, and we adopt $\alpha_s(m_c) = 0.26$ as in Ref. [27, 28]. $R_{nS}(0)$ is the radial S wave function at the origin, and $R''_{nD}(0)$ is the second derivative of the radial D -wave function at the origin. Within the Gaussian basis space, the analytic formula for $R(0)$ is explicitly presented in the APPENDIX. Table 3 compares the leptonic decay given in Ref. [27] with our results in NR and MNR models.

3.3 Two-photon Decay

The two-photon decay widths are important to identify the potential charmonium states, i.e. $X(3915)$, $Z(3930)$ etc. and the latest $X(4160)$, $X(4350)$. With the first-order QCD radiative corrections [26], the two-photon decay widths of 1S_0 , 3P_0 and 3P_2 explicitly are

$$\Gamma_{\gamma\gamma}(^1S_0) = \frac{3\alpha^2 e_c^4 |R_{nS}(0)|^2}{m_c^2} \left[1 + \frac{\alpha_s(m_c)}{\pi} \left(\frac{\pi^2}{3} - \frac{20}{3}\right)\right], \quad (17)$$

$$\Gamma_{\gamma\gamma}(^3P_0) = \frac{27\alpha^2 e_c^4 |R'_{nP}(0)|^2}{m_c^4} \left[1 + \frac{\alpha_s(m_c)}{\pi} \left(\frac{\pi^2}{3} - \frac{28}{9}\right)\right], \quad (18)$$

$$\Gamma_{\gamma\gamma}(^3P_2) = \frac{36\alpha^2 e_c^4 |R'_{nP}(0)|^2}{5m_c^4} \left[1 - \frac{16}{3} \frac{\alpha_s(m_c)}{\pi}\right], \quad (19)$$

where $R'_{nP}(0)$ is the first derivative of the radial P -wave function at the origin. Our numerical results of two-photon decay widths are shown in Table 4 in comparison with Refs.[28, 30].

Table 2 Experimental and theoretical Charmonium mass spectrum. The masses are in units of MeV, and the * denotes the states used in the optimization of potential parameters. Our full-potential calculation results are listed in comparison with the perturbative results of NR model and its relativized extension GI model [21].

State	Expt. [25]	Ref. [21]		Ours	
		NR	GI	NR	MNR
$\eta_c(1^1S_0)^*$	2980.3 ± 1.2	2982	2975	2990.4	2978.4
$J/\psi(1^3S_1)^*$	3096.916 ± 0.011	3090	3098	3085.1	3087.7
$\eta'_c(2^1S_0)^*$	3637 ± 4	3630	3623	3646.5	3646.9
$\psi'(2^3S_1)^*$	3686.09 ± 0.04	3672	3676	3682.1	3684.7
$\eta'_c(3^1S_0)$		4043	4064	4071.9	4058.0
$\psi'(3^3S_1)^*$	4039 ± 1	4072	4100	4100.2	4087.0
$\eta'_c(4^1S_0)$		4384	4425	4420.9	4391.4
$\psi'(4^3S_1)^*$	4421 ± 4	4406	4450	4439.4	4411.4
$\chi_2(1^3P_2)^*$	3556.20 ± 0.09	3556	3550	3551.4	3559.3
$\chi_1(1^3P_1)^*$	3510.66 ± 0.07	3505	3510	3500.4	3517.7
$\chi_0(1^3P_0)^*$	3414.75 ± 0.31	3424	3445	3351.9	3366.3
$h_c(1^1P_1)^*$	3525.42 ± 0.29	3516	3517	3514.6	3526.9
$\chi_2(2^3P_2)$		3972	3979	3979.8	3973.1
$\chi_1(2^3P_1)$		3925	3953	3933.5	3935.0
$\chi_0(2^3P_0)$		3852	3916	3835.7	3842.7
$h_c(2^1P_1)$		3934	3956	3944.6	3941.9
$\chi_2(3^3P_2)$		4317	4337	4383.4	4352.4
$\chi_1(3^3P_1)$		4271	4371	4317.9	4298.7
$\chi_0(3^3P_0)$		4202	4292	4216.7	4207.6
$h_c(3^1P_1)$		4279	4318	4333.9	4309.7
$\chi_2(4^3P_2)$				4736.7	4703.1
$\chi_1(4^3P_1)$				4620.3	4590.5
$\chi_0(4^3P_0)$				4551.8	4521.7
$h_c(4^1P_1)$				4639.5	4606.7
$\psi_3(1^3D_3)$		3806	3849	3814.6	3812.6
$\psi_2(1^3D_2)$		3800	3838	3807.7	3820.1
$\psi(1^3D_1)^*$	3772.92 ± 0.35	3785	3819	3785.3	3808.8
$\eta_{c2}(1^1D_2)$		3799	3837	3807.3	3815.1
$\psi_3(2^3D_3)$		4167	4217	4182.9	4166.1
$\psi_2(2^3D_2)$		4158	4208	4173.7	4168.7
$\psi(2^3D_1)^*$	4153 ± 3	4142	4194	4150.4	4154.4
$\eta_{c2}(2^1D_2)$		4158	4208	4173.7	4164.9
$\psi_3(3^3D_3)$				4572.5	4526.5
$\psi_2(3^3D_2)$				4558.8	4523.6
$\psi(3^3D_1)$				4525.8	4502.2
$\eta_{c3}(3^1D_2)$				4559.7	4521.4
$\chi_4(1^3F_4)$		4021	4095	4037.4	4024.7
$\chi_3(1^3F_3)$		4029	4097	4044.0	4047.6
$\chi_2(1^3F_2)$		4029	4092	4042.4	4059.7
$h_{c3}(1^1F_3)$		4026	4094	4041.1	4040.8
$\chi_4(2^3F_4)$		4348	4425	4371.1	4344.7
$\chi_3(2^3F_3)$		4352	4426	4374.4	4362.4
$\chi_2(2^3F_2)$		4351	4422	4369.9	4369.8
$h_{c3}(2^1F_3)$		4350	4424	4372.3	4356.8
$\chi_4(3^3F_4)$				4744.4	4684.8
$\chi_3(3^3F_3)$				4747.7	4698.5
$\chi_2(3^3F_2)$				4743.9	4704.2
$h_{c3}(3^1F_3)$				4745.9	4694.3
$\psi_5(1^3G_5)$		4214	4312	4236.9	4213.5
$\psi_4(1^3G_4)$		4228	4320	4250.6	4244.7
$\psi_3(1^3G_3)$		4237	4323	4258.2	4267.4
$\eta_{c4}(1^1G_4)$		4225	4317	4247.1	4237.9

Table 3 Leptonic decay width, in units of keV.

Particle	State	Ref.[27]		Ref.[29]		NR		MNR		Expt.[25]
		Γ_{ee}^0	Γ_{ee}	Γ_{ee}^0	Γ_{ee}	Γ_{ee}^0	Γ_{ee}	Γ_{ee}^0	Γ_{ee}	
J/Ψ	1^3S_1	11.8	6.6	12.13	5.6	3.1	6.0	3.3		$5.6 \pm 0.14 \pm 0.02$
ψ'	2^3S_1	4.29	2.4	5.03	2.3	1.3	2.2	1.2		2.4 ± 0.07
$\psi(4040)$	3^3S_1	2.53	1.42	3.48	1.9	1.0	1.8	0.98		0.86 ± 0.07
$\psi(4415)$	4^3S_1	1.25	0.7	2.63	1.3	0.70	1.3	0.70		0.58 ± 0.07
$\psi(3770)$	1^3D_1	0.055	0.031	0.056	0.089	0.050	0.079	0.044		0.27 ± 0.018
$\psi(4160)$	2^3D_1	0.066	0.037	0.096	0.15	0.084	0.13	0.073		0.83 ± 0.07

Table 4 Two-photon decay width, in units of keV.

State	Ref. [28]	Ref. [30]	NR	MNR	Expt. [25]
1^1S_0	5.5	10.94	7.4	7.5	$6.7^{+0.9}_{-0.8}$
2^1S_0	1.8		3.2	2.9	
3^1S_0			2.9	2.5	
4^1S_0			2.0	1.8	
1^3P_0	2.9	6.38	11	10.8	2.29 ± 0.18
2^3P_0	1.9		7.7	6.7	
3^3P_0			7.9	6.5	
1^3P_2	0.50	0.57	0.29	0.27	0.50 ± 0.03
2^3P_2	0.52		0.43	0.39	
3^3P_2			0.81	0.66	

3.4 Radiative Transition

Because radiative transition is sensitively dependent on the detailed features of the wave functions, it is of great interest to have careful inspection. Besides, it has been noticed that the known M1 rates showing serious disagreement between the previous theoretical calculation [21] and experiment. In our full-potential calculation framework, the wave functions are directly associated with the eigenvectors of Hamiltonian corresponding to the masses. The E1 transition rate between an initial charmonium state i of radial quantum number n_i , orbital angular momentum L_i , spin S_i , and total angular momentum J_i , and a final state f is given by Ref. [31] as

$$\Gamma_{E1} \left(n_i^{2S_i+1} L_{iJ_i} \rightarrow n_f^{2S_f+1} L_{fJ_f} \right) = \frac{4}{3} C_{fi} \delta_{S_i S_f} e_c^2 \alpha |\langle \psi_f | r | \psi_i \rangle|^2 E_\gamma^3 \frac{E_f^{(c\bar{c})}}{M_i^{(c\bar{c})}}, \quad (20)$$

$$\Gamma_{M1} \left(n_i^{2S_i+1} L_{iJ_i} \rightarrow n_f^{2S_f+1} L_{fJ_f} \right) = \frac{4}{3} \frac{2J_f+1}{2L_i+1} e_c^2 \frac{\alpha}{m_c^2} \delta_{L_i L_f} \delta_{S_i, S_f \pm 1} |\langle \psi_f | \psi_i \rangle|^2 E_\gamma^3 \frac{E_f^{(c\bar{c})}}{M_i^{(c\bar{c})}}. \quad (21)$$

In the above formulas, e_c is the charge of c-quark in unit of $|e|$, and M_i, E_f represent the eigen mass of initial state and the total energy of final state respectively. The momentum of the final photon equals $E_\gamma = (M_i^2 - M_f^2)/(2M_i)$ in the nonrelativistic approximation [32]. The angular matrix element C_{fi} is

$$C_{fi} = \max(L_i, L_f) (2J_f + 1) \left\{ \begin{matrix} L_f & J_f & S \\ J_i & L_i & 1 \end{matrix} \right\}^2. \quad (22)$$

The Gaussian expanded wave functions give rise to the analytic formulas for the overlap integral, i.e. Eq. (A.8), and the transition matrix elements Eq. (A.10). The n_{max} stands for the dimension of Gaussian basis as defined above. The numerical results of E1 transition rates are presented in Table 5 and Table 6, as well as those of M1 transition in Table 7.

Table 5 2S, 3S, 1P and 2P E1 radiative transitions

Initial meson	Final meson	Ref.[21]				Ours				$\Gamma_{expt.}[25]$ [keV]
		E_γ [MeV]	E_γ [MeV]	Γ_{thy} [keV]	Γ_{thy} [keV]	E_γ [MeV]	E_γ [MeV]	Γ_{thy} [keV]	Γ_{thy} [keV]	
		NR	GI	NR	GI	NR	MNR	NR	MNR	
$\psi'(2^3S_1)$	$\chi_2(1^3P_2)$	128	128	38	24	128	123	43	39	26.6 ± 1.1
	$\chi_1(1^3P_1)$	171	171	54	29	177	163	48	38	28.0 ± 1.2
	$\chi_0(1^3P_0)$	261	261	63	26	315	305	34	29	29.2 ± 0.9
$\eta'_c(2^1S_0)$	$h_c(1^1P_1)$	111	119	49	36	130	118	72	56	
$\psi'(3^3S_1)$	$\chi_2(1^3P_2)$	455	508	0.70	12.7	512	494	6	6.44	< 1.4
	$\chi_1(1^3P_1)$	494	547	0.53	0.85	556	530	0.76	0.44	< 0.9
	$\chi_0(1^3P_0)$	577	628	0.27	0.63	680	657	8.9	8.1	
$\eta'_c(3^1S_0)$	$h_c(1^1P_1)$	485	511	9.1	28	519	496	6.1	7.7	
$\chi_2(1^3P_2)$	$J/\psi(1^3S_1)$	429	429	424	313	436	440	421	405	384.2 ± 16
$\chi_1(1^3P_1)$		390	389	314	239	391	404	330	341	295.8 ± 13
$\chi_0(1^3P_0)$		303	303	152	114	256	267	97	104	119.5 ± 8
$h_c(1^1P_1)$	$\eta_c(1^1S_0)$	504	496	498	352	485	506	465	473	
$\chi_2(2^3P_2)$	$\psi'(2^3S_1)$	276	282	304	207	287	278	300	264	
$\chi_1(2^3P_1)$		232	258	183	183	243	242	243	234	
$\chi_0(2^3P_0)$		162	223	64	135	151	155	77	83	
$h_c(2^1P_1)$	$\eta'_c(2^1S_0)$	285	305	280	218	287	284	297	274	
$\chi_2(2^3P_2)$	$J/\psi(1^3S_1)$	779	784	81	53	794	787	108	111	
$\chi_1(2^3P_1)$		741	763	71	14	757	756	27	33	
$\chi_0(2^3P_0)$		681	733	56	1.3	677	681	30	28	
$h_c(2^1P_1)$	$\eta_c(1^1S_0)$	839	856	140	85	839	846	104	116	
$\chi_2(2^3P_2)$	$\psi_3(1^3D_3)$	163	128	88	29	162	157	81	76	
	$\psi_2(1^3D_2)$	168	139	17	5.6	168	150	14	10	
	$\psi(1^3D_1)$	197	204	1.9	1.0	190	161	0.98	0.64	
$\chi_1(2^3P_1)$	$\psi_2(1^3D_2)$	123	113	35	18	124	113	37	30	
	$\psi(1^3D_1)$	152	179	22	21	145	124	16	11	
$\chi_0(2^3P_0)$	$\psi(1^3D_1)$	81	143	13	51	50	34	4.2	1.4	
$h_c(2^1P_1)$	$\eta_{2c}(1^1D_2)$	133	117	60	27	135	125	61	51	

4 Discussion

4.1 $\psi(3686)$, $\psi(3770)$, $\psi(4160)$

The world-average $\Gamma_{ee}(\psi(3770))$ is 0.265 ± 0.018 keV [25]. The significant leptonic width implies that there is a sizeable S-D mixing between the 2^3S_1 and 1^3D_1 state, since it is expected to be highly suppressed if $\psi(3770)$ is a pure D-wave state (shown in Table 3). The mixing arises both from the usual relativistic correction terms and coupling to strong decay channels, and will affect the E1 transition rates of $\psi(3770)$ and $\psi(3686)$ [32]. We investigate the mixing under the present calculation framework from two scenarios respectively: electronic annihilation and dipole transition. Assuming the $\psi(3686)$ and $\psi(3770)$ to be a mixture of a 1^3D_1 and a 2^3S_1 state as

$$\begin{aligned}
 |\psi(3686)\rangle &= |2^3S_1\rangle \cos\theta - |1^3D_1\rangle \sin\theta, \\
 |\psi(3770)\rangle &= |2^3S_1\rangle \sin\theta + |1^3D_1\rangle \cos\theta.
 \end{aligned} \tag{23}$$

Then, Eqs. (15, 16) can be expressed as

$$\Gamma_{ee}(\psi(3686)) = \frac{4\alpha^2 e_c^2}{M_{\psi'}^2} \left| R_{2S}(0) \cos\theta - \frac{5}{2\sqrt{2}m_c^2} R_{1D}''(0) \sin\theta \right|^2, \tag{24}$$

$$\Gamma_{ee}(\psi(3770)) = \frac{4\alpha^2 e_c^2}{M_{\psi''}^2} \left| R_{2S}(0) \sin\theta + \frac{5}{2\sqrt{2}m_c^2} R_{1D}''(0) \cos\theta \right|^2. \tag{25}$$

Through the fitting of the ratio $\Gamma(\psi(3770) \rightarrow e^+e^-)/\Gamma(\psi(3686) \rightarrow e^+e^-)$, combining the experimental data [25] and the radial wave function values at the origin, i.e. $R_{2S}(0) = 0.556$ GeV^{3/2} and

Table 6 3P, 1D and 2D E1 radiative transitions

Initial meson	Final meson	Ref. [21]				Ours				$\Gamma_{expt.}$ [25] [keV]
		E_γ [MeV] NR	GI	Γ_{thy} [keV] NR	GI	E_γ [MeV] NR	MNR	Γ_{thy} [keV] NR	MNR	
$\chi_2(3^3P_2)$	$\psi(3^3S_1)$	268	231	509	199	273	257	434	360	
$\chi_1(3^3P_1)$		225	212	303	181	212	206	292	272	
$\chi_0(3^3P_0)$		159	188	109	145	115	119	63	72	
$h_c(3^1P_1)$	$\eta_c(3^1S_0)$	229	246	276	208	254	244	377	332	
$\chi_2(3^3P_2)$	$\psi'(2^3S_1)$	585	602	55	30	645	617	112	97	
$\chi_1(3^3P_1)$		545	585	45	8.9	589	570	30	31	
$\chi_0(3^3P_0)$		484	563	32	0.045	501	490	25	19	
$h_c(3^1P_1)$	$\eta'_c(2^1S_0)$	593	627	75	43	633	612	95	90	
$\chi_2(3^3P_2)$	$J/\psi(1^3S_1)$	1048	1063	34	19	1106	1081	62	59	
$\chi_1(3^3P_1)$		1013	1048	31	2.2	1057	1040	10	11	
$\chi_0(3^3P_0)$		960	1029	27	1.5	980	971	23	22	
$h_c(3^1P_1)$	$\eta_c(1^1S_0)$	1103	1131	72	38	1135	1126	73	76	
$\chi_2(3^3P_2)$	$\psi_3(2^3D_3)$	147	118	148	51	196	182	279	231	
	$\psi_2(2^3D_2)$	156	128	31	9.9	205	180	48	34	
	$\psi(2^3D_1)$	155	141	2.1	0.77	227	194	3.2	2.1	
$\chi_1(3^3P_1)$	$\psi_2(2^3D_2)$	112	108	58	35	142	128	121	92	
	$\psi(2^3D_1)$	111	121	19	15	164	142	50	34	
$\chi_0(3^3P_0)$	$\psi(2^3D_1)$	43	97	4.4	35	66	53	21	11	
$h_c(3^1P_1)$	$\eta_{2c}(2^1D_2)$	119	109	99	48	157	142	205	158	
$\chi_2(3^3P_2)$	$\psi_3(1^3D_3)$	481	461	0.049	6.8	532	506	1.6	1.4	
	$\psi_2(1^3D_2)$	486	470	0.0091	0.13	538	500	0.76	0.42	
	$\psi(1^3D_1)$	512	530	0.00071	0.001	557	510	0.11	0.062	
$\chi_1(3^3P_1)$	$\psi_2(1^3D_2)$	445	452	0.035	4.6	480	452	1.2	1.8	
	$\psi(1^3D_1)$	472	512	0.014	0.39	500	462	0.11	0.00029	
$\chi_0(3^3P_0)$	$\psi(1^3D_1)$	410	490	0.037	9.7	409	380	28	30	
$h_c(3^1P_1)$	$\eta_{2c}(1^1D_2)$	453	454	0.16	5.7	495	466	0.21	0.56	
$\psi_3(1^3D_3)$	$\chi_2(1^3P_2)$	242	282	272	296	254	245	340	302	
$\psi_2(1^3D_2)$	$\chi_2(1^3P_2)$	236	272	64	66	248	252	79	82	
	$\chi_1(1^3P_1)$	278	314	307	268	295	290	321	301	
$\psi(1^3D_1)$	$\chi_2(1^3P_2)$	208	208	4.9	3.3	227	241	6.8	8.1	< 24.6
	$\chi_1(1^3P_1)$	250	251	125	77	274	280	146	153	79.2 ± 16
	$\chi_0(1^3P_0)$	338	338	403	213	409	417	367	362	199.3 ± 25
$h_c(1^1D_2)$	$h_c(1^1P_1)$	264	307	339	344	281	277	398	374	
$\psi_3(2^3D_3)$	$\chi_2(1^3P_2)$	566	609	29	16	584	563	23	23	
$\psi_2(2^3D_2)$	$\chi_2(1^3P_2)$	558	602	7.1	0.62	576	565	0.85	1.5	
	$\chi_1(1^3P_1)$	597	640	26	23	619	600	38	41	
$\psi(2^3D_1)$	$\chi_2(1^3P_2)$	559	590	0.79	0.027	556	552	0.18	0.080	< 1.3
	$\chi_1(1^3P_1)$	598	628	14	3.4	599	588	3.6	5.5	< 0.7
	$\chi_0(1^3P_0)$	677	707	27	35	722	713	99	109	
$h_c(2^1D_2)$	$h_c(1^1P_1)$	585	634	40	25	607	589	38	41	

$R''_{1D}(0) = 0.144 \text{ GeV}^{7/2}$, we find two solutions for the mixing angle:

$$\theta = 8^\circ \pm 0.4^\circ \quad \text{or} \quad \theta = -30^\circ \pm 0.4^\circ. \quad (26)$$

These solutions are smaller than $(12 \pm 2)^\circ$ or $-(27 \pm 2)^\circ$ determined by leptonic decay widths in [35, 27], partially due to more precise measurements. Impending, we illustrate the mixing-dependency of E1 transitions of our model in Fig. 1 and Fig. 2. The decay widths of $\psi(3686) \rightarrow \gamma\chi_{c0}, \gamma\chi_{c1}$ obviously favor $\theta = 8^\circ$, while the matching angle for $\gamma\chi_{c2}$ locates around $\theta = -30^\circ$ and $\theta = 50^\circ$. The $\theta = 50^\circ$ would be too large for the two states mixing. On the other hand, a positive and slight mixing is compatible for $\psi(3770) \rightarrow \gamma\chi_{c0}, \gamma\chi_{c2}$ consisting with $\theta = 8^\circ$, except the challenging $\gamma\chi_{c1}$ fitting with a small but negative angle. This discrepancy reveals that S - D wave mixing would be important for $\psi(3770)$ and $\psi(3686)$, but not sufficient. The mixing-angle functions for the two out-standing decays

Table 7 M1 radiative partial widths

Initial meson	Final meson	Ref. [21]				Ours				$\Gamma_{expt.}$ [keV]
		E_γ [MeV] NR	GI	Γ_{thy} [keV] NR	GI	E_γ [MeV] NR	MNR	Γ_{thy} [keV] NR	MNR	
$J/\psi(1^3S_1)$	$\eta_c(1^1S_0)$	116	115	2.9	2.4	93	107	1.5	2.2	1.58 ± 0.37 [25]
$\psi'(2^3S_1)$	$\eta'_c(2^1S_0)$	48	48	0.21	0.17	35	38	0.086	0.096	$0.143 \pm 0.027 \pm 0.092$ [33]
		639	638	4.6	9.6	627	639	3.1	3.8	0.97 ± 0.14 [34]
$\eta'_c(2^1S_0)$	$J/\psi(1^3S_1)$	501	501	7.9	5.6	518	516	6.1	6.9	
$\psi(3^3S_1)$	$\eta_c(3^1S_0)$	29	35	0.046	0.067	28	29	0.043	0.044	
	$\eta'_c(2^1S_0)$	382	436	0.61	2.6	429	416	0.70	0.71	
	$\eta_c(1^1S_0)$	922	967	3.5	9.0	960	958	3.2	3.7	
$\eta_c(3^1S_0)$	$\psi'(2^3S_1)$	312	361	1.3	0.84	371	356	1.7	1.6	
	$J/\psi(1^3S_1)$	810	856	6.3	6.9	867	854	5.9	6.5	
$h'_c(2^1P_1)$	$\chi_2(1^3P_2)$	360	380	0.071	0.11	374	364	1.3	1.2	
	$\chi_1(1^3P_1)$	400	420	0.058	0.36	419	401	0.16	0.13	
	$\chi_0(1^3P_0)$	485	504	0.033	1.5	548	534	5.6	5.3	
$\chi_2(2^3P_2)$	$h_c(1^1P_1)$	430	435	0.067	1.3	438	421	1.0	0.89	
$\chi_1(2^3P_1)$	$h_c(1^1P_1)$	388	412	0.050	0.045	397	387	0.15	0.13	
$\chi_0(2^3P_0)$	$h_c(1^1P_1)$	321	379	0.029	0.50	308	303	4.8	4.8	
$h'_c(3^1P_1)$	$\chi_2(2^3P_2)$					340	323	1.7	1.5	
	$\chi_1(2^3P_1)$					382	358	0.17	0.12	
	$\chi_0(2^3P_0)$					470	442	3.5	2.7	
	$\chi_2(1^3P_2)$					712	685	2.3	2.1	
	$\chi_1(1^3P_1)$					753	719	0.27	0.22	
	$\chi_0(1^3P_0)$					871	840	8.9	8.2	
$\chi_2(3^3P_2)$	$h_c(2^1P_1)$					417	391	1.2	0.99	
	$h_c(1^1P_1)$					783	747	1.8	1.5	
$\chi_1(3^3P_1)$	$h_c(2^1P_1)$					357	342	0.16	0.12	
	$h_c(1^1P_1)$					729	703	0.22	0.20	
$\chi_0(3^3P_0)$	$h_c(2^1P_1)$					263	257	3.7	3.3	
	$h_c(1^1P_1)$					644	626	5.3	5.1	

may be modified by the first-order relativistic corrections to their wave functions, since the relativistic corrections play an essential role in E1 radiative transitions indeed, as suggested in [35].

The S - D mixing may be more serious for the higher charmonium above the open-charm threshold [36, 29, 27, 37]. As shown in Table 3, the experimental leptonic decay width of the $\psi(4160)$ is significantly larger than the potential model predictions as 2^3D_1 . In Ref. [37], it is explored that the possible mixing in $(n+1)^3S_1$ - n^3D_1 determined by the ratio of di-electron widths and get a large mixing angle $\sim 34^\circ$ ($n = 2, 3$), while the hyperfine effects are neglected in the wave functions by a universal potential. In the current framework, the spin-dependent interactions at $\mathcal{O}(v^2/c^2)$ are thoroughly considered to determination of the state wave functions. Besides the distinct leptonic decay widths, it is found that the theoretical E1 radiative rates of the pure 2^3D_1 and 3^3S_1 are incomparable with the available experimental data. This discrepancy seems cannot be eliminated by the relativistic corrections, hence dissimilar with the situations of $\psi(3770)$ and $\psi(3686)$. We extend above pattern to the $\psi(4040)$ - $\psi(4160)$ and $\psi(4160)$ - $\psi(4415)$ mixing scenarios, and also independently via the leptonic decays as well as their E1 radiative rates. Combining the corresponding values of wave functions at the origin, i.e. $R_{3S}(0) = 0.556 \text{ GeV}^{3/2}$, $R_{4S}(0) = 0.508 \text{ GeV}^{3/2}$ and $R_{2D}''(0) = 0.201 \text{ GeV}^{7/2}$ and the central values of experimental data $\Gamma_{ee}(\psi(4040)) = 0.86 \pm 0.07 \text{ keV}$, $\Gamma_{ee}(\psi(4160)) = 0.83 \pm 0.07 \text{ keV}$ and $\Gamma_{ee}(\psi(4415)) = 0.58 \pm 0.07 \text{ keV}$ [25], the mixing angles determined by the leptonic decay widths are listed in Table 8.

In Fig.3, one can figure out that the mixing angles given by the Γ_{ee} , i.e. 29.8° or -60.7° , are still acceptable for the E1 transitions. Then, it is in a dilemma that the $\Gamma(\psi(4040) \rightarrow \gamma\chi_{c1})$ and $\Gamma(\psi(4160) \rightarrow \gamma\chi_{c2})$ favor $\theta = 29.8^\circ$, while $\Gamma(\psi(4040) \rightarrow \gamma\chi_{c2})$ and $\Gamma(\psi(4160) \rightarrow \gamma\chi_{c1})$ support $\theta = -60.7^\circ$. Both of the two solutions seems to be equally important, and it is difficult to rule out any one of them from the current perspective, possibly due to the mixing model being oversimplified. Nevertheless,

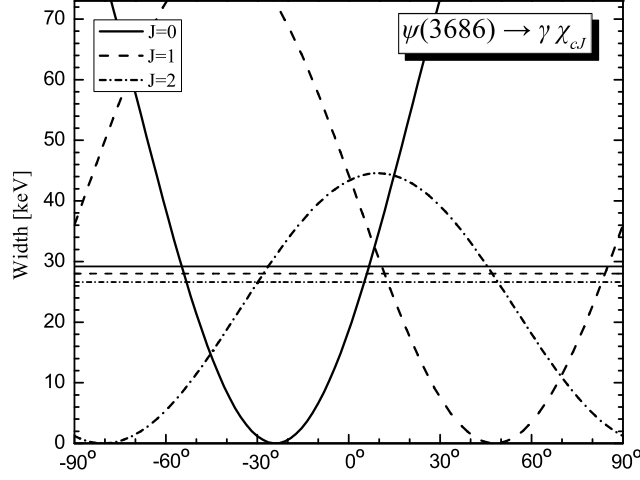


Fig. 1 The E1 radiative transition rate of $\psi(3686) \rightarrow \gamma 1^3P_J$ dependent on the various mixing angle θ . Because of the relatively precise and very close measurements for the three channels, we illustrate the central values of $\Gamma_{expt.}$ [25] with single lines rather than the error-associated areas.

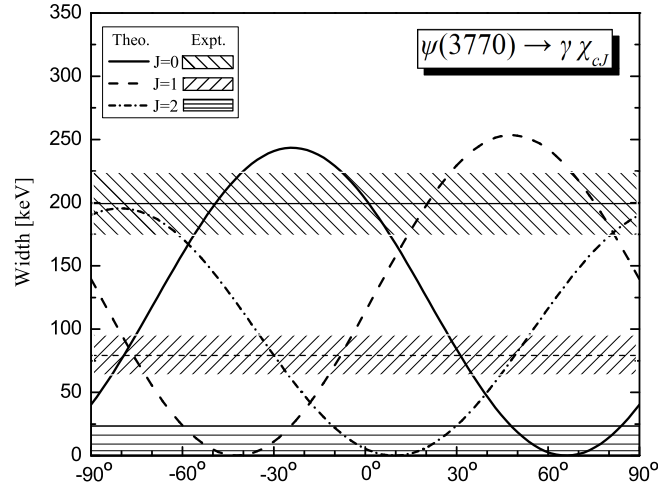


Fig. 2 The E1 radiative transition rate of $\psi(3770) \rightarrow \gamma 1^3P_J$ dependent on the various mixing angle θ . The experimental data [25] are illustrated by the central values as well as the related errors.

Table 8 The 3^3S_1 - 2^3D_1 and 4^3S_1 - 2^3D_1 mixing for the higher charmonium di-electron decays. Our predictions are obtained with the MNR potential model. Since the inverse definitions about mixing angle, these assignments in Ref. [36] are reasonably exchanged here for a proper comparison.

Mixing states	Ref.[36]	Mixing angle Ref.[37]	Ours
$3S$ - $2D$	$35^\circ / -55^\circ$	$34.8^\circ / -55.7^\circ$	$29.8^\circ / -60.7^\circ$
$4S$ - $2D$			$24.8^\circ / -58.5^\circ$

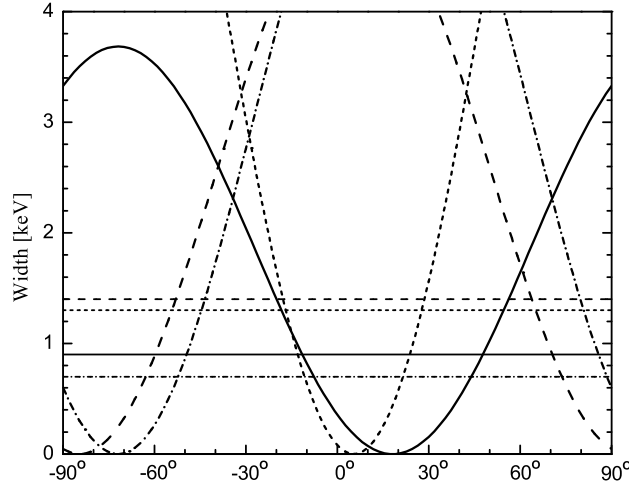


Fig. 3 The mixing angle θ -dependent E1 radiative transition rates of $\psi(4040) \rightarrow \gamma\chi_{c1}$ (solid), $\psi(4040) \rightarrow \gamma\chi_{c2}$ (dash), $\psi(4160) \rightarrow \gamma\chi_{c1}$ (short dash dot) and $\psi(4160) \rightarrow \gamma\chi_{c2}$ (short dash). The experimental upper limits [25] are represented in the same line-shape with the corresponding channels.

it would be still interesting to glean something for the further understandings and revisiting with more precise measurements.

4.2 $X(3872)$ and $X(3915)$

The first surprising charmonium-like state $X(3872)$ [38] is still far away from sufficiently understanding. Its quantum numbers have not been decided yet from $J^{PC} = 1^{++}$ and $J^{PC} = 2^{-+}$ [39]. The radiative decay $\gamma J/\psi$ [40, 41] bolsters the 1^{++} assignment, while the $J^P = 2^-$ is ratherish favored by a study of the 3π invariant mass distribution in $J/\psi\omega$ decays [42, 2]. Assuming the charmonium structure, these J^{PC} imply the possible candidates, i.e. $\chi_{c1}(2^3P_1)$ and $\eta_{c2}(1^1D_2)$. As the spectrum listed in Table 2, the masses of the two states remain a gap around 50 MeV with the world-average mass $M = 3871.56 \pm 0.22$ MeV [25]. Combining the observed branching fraction [40] and the full width, it is evaluated that the radiative decay widths are $\Gamma(X(3872) \rightarrow J/\psi\gamma) > 20.7$ keV and $\Gamma(X(3872) \rightarrow \psi(2S)\gamma) > 0.069$ MeV. The theoretical results of the radiative decays for the conventional charmonium candidates are apparently too large, and the ratio of the two rates is nearly two times larger than the observation. Hence, the $c\bar{c}$ nature of $X(3872)$ seems unlikely in the present framework.

Another interesting resonance named $X(3915)$ has been announced by Belle Collaboration [43], which is found in the processes $\gamma\gamma \rightarrow J/\psi\omega$. $X(3915)$ clearly has the positive C -parity, but the J^P assignment remains to be determined. Owing to the same production and decay signatures, the $Y(3940)$ [44, 45] and the $X(3915)$ are considered to be the same state prevalingly, which is close to those of the $Z(3930)$. If the $Z(3930)$ (discussed in the coming section) occupies the assignment of χ'_{c2} [7, 46], the possibility of $X(3915)$ can be ruled out, or else they are the same state as $\chi_{c2}(2^3P_2)$. The world-average mass and width of the $X(3915)$ are $M = 3917.4 \pm 2.7$ MeV, $\Gamma = 28_{-9}^{+10}$ MeV [25]. In our predictions, the mass of $\chi_{c2}(2^3P_2)$ is about 60 MeV higher than the experimental data for the $X(3915)$. Even if the mass is roughly plausible, the conventional $c\bar{c}$ structure of $X(3915)$ would likely encounter trouble in accommodating the product of the two-photon decay width and the branching ratio to $J/\psi\omega$, i.e. $\Gamma(\gamma\gamma) \times \mathcal{B}(X(3915) \rightarrow J/\psi\omega) = 61 \pm 17 \pm 8$ eV for $J^P = 0^+$ and $18 \pm 5 \pm 2$ eV for $J^P = 2^+$. As shown in Table 4, the two-photon decay width is $\Gamma_{\gamma\gamma}(2^3P_2) = 0.39$ keV in the MNR potential model. Based on the central value of the world-average width, $\Gamma(X(3915) \rightarrow J/\psi\omega)$ is expected to be 1.29 MeV ($J^{PC} = 2^+$) or 4.38 MeV ($J^{PC} = 0^+$) approximately, which is over ten times larger than that of the typical charmonium. On the other hand, the charmonium candidate $\chi_{c0}(2^3P_0)$

with $J^P = 0^{++}$ may be slightly better in $\Gamma(\gamma\gamma)$, but worse in mass spectrum. The strong-decay inspection of the $X(3915)$ also disfavor the structure as $\chi_{c0}(2^3P_0)$ [47, 48]. It has been interpreted as the multiquark and molecule state [49, 50, 51]. So far, the nature of $X(3915)$ is still murky, and the charmonium system have seemed inefficient to provide a consensus of interpretation.

4.3 $X(3940)$ and $Z(3930)$

The $X(3940)$ was seen by the Belle Collaboration in the recoiling spectrum of J/ψ in the e^+e^- annihilation process [52]. The mass and width of $X(3940)$ are $M = 3942_{-6}^{+7} \pm 6$ MeV, $\Gamma = 37_{-15}^{+26} \pm 8$ MeV [25]. This state is not seen to decay into $D\bar{D}$ but does decay into $D\bar{D}^*$, suggesting that it has unnatural parity and can be a candidate for the $\eta_c(3^1S_0)$. The predicted mass is much higher by the potential models [21, 27, 20, 23], including the present work. Taking the coupling channel effect into account [53], the induced spin-spin splitting between 3^3S_1 and 3^1S_0 will be increased and consequently lower down the mass of 3^1S_0 state. We predicate the radiative transitions and two-photon decay width of 3^1S_0 for testing the nature of $X(3940)$ as the charmonium candidate.

The Belle Collaboration has observed $Z(3930)$ state [54] in two-photon fusion, $\gamma\gamma \rightarrow Z(3930) \rightarrow DD$. The world-average mass and full width are $M = 3927.2 \pm 2.6$ MeV, $\Gamma = 24 \pm 6$ MeV [25]. And the theoretical prediction of mass within our framework is almost the same as the perturbative results, nearly 40 MeV higher than the observation. Due largely to the agreement with the detected angular distribution [54, 55] for $J = 2$ and to the plausible mass of a $2P$ $c\bar{c}$ state, $Z(3930)$ is now widely accepted as $\chi_{c2}(3930)$ [56, 57, 25, 7, 54]. The value of the partial width $\Gamma(\gamma\gamma) \times \mathcal{B}(Z(3930) \rightarrow D\bar{D}) = 0.24 \pm 0.05 \pm 0.04$ keV was found in the Babar experiment [55]. Our prediction of $\Gamma(\gamma\gamma)$ is 0.39 keV and 0.43 keV within the MNR model and the NR model respectively. With the theoretical open-charm strong decay width $\Gamma(Z(3930) \rightarrow D\bar{D}) = 21.5$ MeV [56], one can directly evaluate $\Gamma(\gamma\gamma) \approx 0.27 \pm 0.07$ keV. Our prediction of the two-photon width for $\chi_{c2}(2^3P_2)$ is reasonably consistent with this estimation, supporting $Z(3930)$ assigned as charmonium 2^3P_2 .

4.4 $X(4160)$

The Belle Collaboration has reported the $X(4160)$ in the process $e^+e^- \rightarrow J/\psi D^* \bar{D}^*$ with a significance of 5.1σ [58]. Its mass and width are $M = 4156_{-20}^{+25} \pm 15$ MeV and $\Gamma = 139_{-61}^{+111} \pm 21$ MeV respectively. Since within this process e^+e^- annihilate into one photon, the charge parity of $X(4160)$ should be $C = +$. The possible interpretation of its structure from the view of the production rate in $e^+e^- \rightarrow J/\psi X(4160)$ favors the candidate $\chi_{c0}(3^3P_0)$ [36], although the predicted mass differs around 30 MeV in the color screened potential model [27]. In our calculated spectrum shown in Table 2, our prediction of $\eta_c(2^1D_2)$ is $M(2^1D_2) = 4164.9$ MeV in MNR model and 4173.7 MeV in NR model. It is suggested that $X(4160)$ can be excellently reproduced by the charmonium spectrum as $\eta_c(2^1D_2)$ in our calculation framework. Investigating the strong decay properties of $X(4160)$, Ref. [47] has indicated that the decay width of $\eta_c(2^1D_2)$ agrees well with the Belle data of $X(4160)$, which includes the absence of theoretical forbidden channel $\eta_c(2^1D_2) \rightarrow D\bar{D}$. Other possible candidates, i.e. $\chi_{c0}(3^3P_0)$, $\chi_{c1}(3^3P_1)$, $\eta_c(4^1S_0)$ are disfavored from this perspective. The charmonium structure of $X(4160)$ as $\eta_c(2^1D_2)$ can be further explored by electromagnetic transition rates, which have been predicted in this paper as well.

4.5 $X(4350)$

The $X(4350)$ found in the invariant mass spectrum of $J/\psi\phi$ by the Belle Collaboration [59], is of $M = 4350_{-5.1}^{+4.6} \pm 0.7$ MeV and $\Gamma = 13.3_{-9.1}^{+17.9} \pm 4.1$ MeV. Its assignment J^{PC} could be 0^{++} or 2^{++} . As a new charmonium-like state, so far, it has been interpreted as P -wave charmonium state [60, 48], the $D_s^* D_{s0}^*$ molecule [61, 62], the $c\bar{c}s\bar{s}$ state [63] and a mixture of scalar $c\bar{c}$ and $D_s^* \bar{D}_s^*$ [64] etc.. In particular, Ref. [60] has presented the open-charm decay behaviors of the possible $c\bar{c}$ options, i.e. $\chi_{cJ}(3P)$ ($J = 0, 1, 2$), using the quark pair creation (QPC) model. Only the decay properties of $\chi_{c2}(3^3P_2)$ are consistent with the existing experimental data on the $X(4350)$. Besides, the hidden charm decay $\Gamma(X(4350) \rightarrow J/\psi\phi)$ [48] via $D\bar{D}^{(*)}$ intermediate states favors the assignment being P -wave charmonium as well.

The mass of $\chi_{c2}(3^3P_2)$ in our calculation is 4383.4 MeV (NR) and 4352.4 MeV (MNR). Consequently, the quantum number of the $X(4350)$ is reasonably favored as $J^{PC} = 2^{++}$ with the charmonium state $\chi_{c2}(3^3P_2)$ from the current exact mass prediction and strong decay behavior. To confirm this new member of charmonium family, more experimental data are required. We provide the corresponding radiative transition rates (see Table 6 for E1 channels and Table 7 for M1) and the two-photon decay width $\Gamma_{\gamma\gamma}(3^3P_2) = 0.66$ keV for the further testing.

4.6 M1 transition of J/ψ and ψ'

A well-known problem is evident in the decay rate of $J/\psi \rightarrow \gamma\eta_c$, which is that the predicted rate in the nonrelativistic potential model is about a factor of 2-3 larger than experiment in the previous calculations[21, 29]. Since this rate only involves the charm quark magnetic moment, this discrepancy leads to a surprise. When we adopt the wave functions generated from the full-potential Hamiltonian, this unexpected discrepancy seems can be reduced.

The radiative transition rates of ψ' from the previous perturbative calculation, both NR model and GI model, have showed serious disagreement with theory. Particularly, the predicted partial decay width of $\psi' \rightarrow \gamma\eta_c$ was nearly one order of magnitude larger than the experimental observation [25]. The lattice QCD calculation [65] obtained $\psi' \rightarrow \gamma\eta_c = 0.4 \pm 0.8$ keV, while its uncertainty was apparently large. Recently, Li and Zhao has interpreted this discrepancy of potential model via taking the intermediate meson loop (IML) into account [66]. The IML contributions bring down the GI amplitude to $2.05^{+2.650}_{-1.75}$ keV, where the cut-off parameter played a crucial and sensitive role. Besides, the uncertainties from IML also due to the radiative couplings. We re-examined the NR model through the full-potential calculation, and found $\Gamma(\psi' \rightarrow \gamma\eta_c) = 3.1$ keV (see Table 7). In comparison with the perturbative results, the present approach may obtain a better wave function. For $\psi' \rightarrow \gamma\eta'_c$, our prediction is also in a reasonable agreement with the first measurement [33] of this decay channel by BES-III Collaboration very recently.

5 Remarks

By mean of a proper variational method, we calculate precisely the eigen value and eigen function of the Hamiltonian including the full interactions, which might maintain the subtleness of wave functions. We investigate the mass spectrum, electromagnetic transitions, leptonic decays and two-photon widths of the charmonium states. Comparing the results from the pure scalar and the scalar-vector mixing linear confinement, it is revealed that the mixture might be important for reproducing the mass spectrum and decay widths. Explicitly, about 22% vector component is obtained via optimizing the potential parameters. The scalar-vector mixing model requires less linear slope, and more in the spin-splitting than the pure scalar confinement. In our calculations, the M1 radiative transitions rates of J/ψ and ψ' is reduced by the obtained wave functions actually, consisting with the experimental observations in order. The S - D mixing are explored in the higher charmonium states. To the newly found charmonium-like states, we perform a reasonable inspection of the possible $c\bar{c}$ assignments. The $X(4160)$ and $X(4350)$ are found in the mass spectrum as $M(2^1D_2) = 4164.9$ MeV and $M(3^3P_2) = 4352.4$ MeV, which strongly favor the $J^{PC} = 2^{-+}, 2^{++}$ assignments respectively. With the available experimental data, the $Z(3930)$ is favored as $\chi_{c2}(2^3P_2)$, while the $X(3872)$ and $X(3915)$ are disfavored by charmonium states. The corresponding radiative transitions, leptonic and two-photon decay widths of the $X(3940)$, $X(4160)$ and $X(4350)$ have been calculated for the further experimental search and identifying the new members of charmonium family.

Acknowledgements This work was supported in part by the National Natural Science Foundation of China (No.11175146, No.11047023) and the Fundamental Research Funds for the Central Universities (No.XDJK2012D005).

Appendix: Wave functions and matrix elements for Gaussian basis expansion

Since the state wave function $\psi_{lm}(\mathbf{r})$ are expanded in the Gaussian basis space, the Hamiltonian matrix elements and the radial wave function at the origin, as well as the overlap integral involved in

the transition matrix elements are explicitly analytic. We present these formulas used in the numerical calculation of the mass and decay width as follows.

$$\langle \phi_{nlm}^G | \frac{1}{r} | \phi_{n'l'm'}^G \rangle = \frac{2}{\sqrt{\pi}} \frac{2^l l!}{(2l+1)!!} \sqrt{v_n + v_{n'}} \left(\frac{2\sqrt{v_n v_{n'}}}{v_n + v_{n'}} \right)^{l+\frac{3}{2}} \quad (\text{A.1})$$

$$\langle \phi_{nlm}^G | r | \phi_{n'l'm'}^G \rangle = \frac{2^{l+1}}{\sqrt{\pi}} \frac{(l+1)!}{(2l+1)!!} \frac{1}{\sqrt{v_n + v_{n'}}} \left(\frac{2\sqrt{v_n v_{n'}}}{v_n + v_{n'}} \right)^{l+\frac{3}{2}} \quad (\text{A.2})$$

$$\langle \phi_{nlm}^G | e^{-\sigma^2 r^2} | \phi_{n'l'm'}^G \rangle = \left(\frac{2\sqrt{v_n v_{n'}}}{v_n + v_{n'} + \sigma^2} \right)^{l+\frac{3}{2}} \quad (\text{A.3})$$

$$\langle \phi_{nlm}^G | \frac{1}{r^3} | \phi_{n'l'm'}^G \rangle = \frac{2^{l+1}}{\sqrt{\pi}} \frac{(l-1)!}{(2l+1)!!} (v_n + v_{n'})^{\frac{3}{2}} \left(\frac{2\sqrt{v_n v_{n'}}}{v_n + v_{n'}} \right)^{l+\frac{3}{2}} \quad (\text{A.4})$$

$$R_{nS}(0) = \sum_{x=1}^{n_{max}} \frac{2 \times 2^{3/4} \sqrt{v_x^{3/2}}}{\pi^{1/4}} \quad (\text{A.5})$$

$$R_{nD}''(0) = \sum_{x=1}^{n_{max}} \frac{16 \times 2^{3/4} \sqrt{v_x^{7/2}}}{\sqrt{15} \pi^{1/4}} \quad (\text{A.6})$$

$$R_{nP}'(0) = \sum_{x=1}^{n_{max}} \frac{4 \times 2^{3/4} \sqrt{v_x^{5/2}}}{\sqrt{3} \pi^{1/4}} \quad (\text{A.7})$$

$$\langle \psi_f | r | \psi_i \rangle = \int_0^\infty \psi_f(\mathbf{r}) r \psi_i(\mathbf{r}) r^2 dr = \sum_{x=1}^{n_{max}} \sum_{y=1}^{n_{max}} C_{xL_i} C_{yL_f} \langle \phi_{yL_f}^G | r | \phi_{xL_i}^G \rangle \quad (\text{A.8})$$

$$\langle \psi_f | \psi_i \rangle = \int_0^\infty \psi_f(\mathbf{r}) \psi_i(\mathbf{r}) r^2 dr = \sum_{x=1}^{n_{max}} \sum_{y=1}^{n_{max}} C_{xL_i} C_{yL_f} \langle \phi_{yL_f}^G | \phi_{xL_i}^G \rangle \quad (\text{A.9})$$

$$\langle \phi_{yL_f}^G | r | \phi_{xL_i}^G \rangle = \frac{2^{\frac{5}{2}+L_f+L_i} \sqrt{v_y^{L_f+\frac{3}{2}} v_x^{L_i+\frac{3}{2}}}}{\sqrt{\pi} \sqrt{(2L_f+1)!!(2L_i+1)!!}} (v_y + v_x)^{\frac{1}{2}(-L_f-L_i-4)} \Gamma \left[\frac{1}{2}(L_f + L_i + 4) \right] \quad (\text{A.10})$$

$$\langle \phi_{yL_f}^G | \phi_{xL_i}^G \rangle = \frac{2^{\frac{5}{2}+L_f+L_i} \sqrt{v_y^{L_f+\frac{3}{2}} v_x^{L_i+\frac{3}{2}}}}{\sqrt{\pi} \sqrt{(2L_f+1)!!(2L_i+1)!!}} (v_y + v_x)^{\frac{1}{2}(-L_f-L_i-3)} \Gamma \left[\frac{1}{2}(L_f + L_i + 3) \right] \quad (\text{A.11})$$

References

1. Brambilla N, et al. (Quarkonium Working Group) (2011) Heavy quarkonium: progress, puzzles, and opportunities. Eur. Phys. J. C71: 1534, arXiv:1010.5827 [hep-ph]
2. Biassoni P (2010) Recent results in charmonium spectroscopy at B-factories. arXiv:1009.2627 [hep-ex]
3. Voloshin M (2008) Review charmonium. Prog. Part. Nucl. Phys. 61: 455-511
4. Eichten E, Gottfried K, Kinoshita T, Lane K D, Yan T M (1976) Interplay of confinement and decay in the spectrum of charmonium. Phys. Rev. Lett. 36: 500-504
5. Eichten E, Gottfried K, Kinoshita T, Lane K D, Yan T M (1978) Charmonium: The model. Phys. Rev. D 17: 3090-3117
6. Eichten E, Gottfried K, Kinoshita T, Lane K D, Yan T M (1980) Charmonium: Comparison with experiment. Phys. Rev. D 21: 203-233
7. Godfrey S, Isgur N (1985) Mesons in a relativized quark model with chromodynamics. Phys. Rev. D 32: 189-231
8. Stanley D P, Robson D (1980) Nonperturbative potential model for light and heavy quark-antiquark systems. Phys. Rev. D 21: 3180-3196

9. Ebert D, Faustov R N, Galkin V O (2003) Properties of heavy quarkonia and bc mesons in the relativistic quark model. Phys. Rev. D 67: 014027
10. Gershtein S S, Kiselev V V, Likhoded A K, Tkabladze A V (1995) B_c spectroscopy. Phys. Rev. D 51: 3613-3627
11. Fulcher L P (1991) Perturbative QCD, a universal QCD scale, long-range spin-orbit potential, and the properties of heavy quarkonia. Phys. Rev. D 44: 2079-2084
12. Fulcher L P (1999) Phenomenological predictions of the properties of the B_c system. Phys. Rev. D 60: 074006
13. Fulcher L P (1994) Matrix representation of the nonlocal kinetic energy operator, the spinless salpeter equation and the cornell potential. Phys. Rev. D 50: 447-453
14. Gupta S N, Johnson J M, Repko W W, Suchyta C J (1994) Heavy quarkonium potential model and the 1P_1 state of charmonium. Phys. Rev. D 49: 1551-1555
15. Gupta SN, Johnson JM (1996) B_c spectroscopy in a quantum-chromodynamic potential model. Phys. Rev. D 53: 312-314
16. Zeng J, Van Orden J W, Roberts W (1995) Heavy mesons in a relativistic model. Phys. Rev. D 52: 5229-5241
17. Eichten E, Gottfried K, Kinoshita T, Lane K D, Yan T M (1978) Charmonium: The model. Phys. Rev. D 17: 3090-3117
18. Eichten E, Gottfried K, Kinoshita T, Lane K D, Yan T M (1980) Erratum: Charmonium: The model. Phys. Rev. D 21: 313
19. Buchmuller W (1982) Fine- and hyperfine structure of quarkonia. Phys. Lett. B 112:479-483
20. Ebert D, Faustov R N, Galkin V O (2000) Quark-antiquark potential with retardation and radiative contributions and the heavy quarkonium mass spectra. Phys. Rev. D 62: 034014
21. Barnes T, Godfrey S, Swanson E S (2005) Higher charmonia. Phys. Rev. D 72: 054026
22. Li B Q, Chao K T (2009) Higher charmonia and X, Y, Z states with screened potential. Phys. Rev. D 79: 094004
23. Radford S F, Repko W W (2007) Potential model calculations and predictions for heavy quarkonium. Phys. Rev. D 75: 074031
24. Hiyama E, Kino Y, Kamimura M (2003) Gaussian expansion method for few-body systems. Prog. Part. Nucl. Phys. 51: 223-307
25. Nakamura K, et al. (Particle Data Group) (2010) The review of particle physics. J. Phys. G 37: 075021, and 2011 partial update for the 2012 edition
26. Kwong W, Mackenzie P B, Rosenfeld R, Rosner J L (1988) Quarkonium annihilation rates. Phys. Rev. D 37:3210-3215
27. Ding Y B, Chao K T, Qin D H (1993) Screened Q-Q potential and spectrum of heavy quarkonium. Chin. Phys. Lett. 10: 460-463
28. Ebert D, Faustov R N, Galkin V O (2003) Two-photon decay rates of heavy quarkonia in the relativistic quark model. Mod. Phys. Lett. A 18: 601-608, arXiv:0302044 [hep-ph]
29. Barnes T (2004) Charmonium at BES and CLEO-c. arXiv:0406327 [hep-ph]
30. Gupta S N, Johnson J M, Repko W W (1996) Relativistic two-photon and two-gluon decay rates of heavy quarkonia. Phys. Rev. D 54: 2075-2080
31. Kwong W, Rosner J L (1988) D-wave quarkonium levels of the Υ family. Phys. Rev. D 38:279-297
32. Brambilla N, et al. (Quarkonium Working Group) (2005) CERN Yellow Report. arXiv:0412158 [hep-ph]
33. Wang L, et al. (BESIII Collaboration) (2011) Study of charmonium spectroscopy at BESIII. arXiv:1110.2560 [hep-ex]
34. Mitchell R, et al. (CLEO Collaboration) (2009) J/ψ and $\psi(2S)$ radiative decays to η_c . Phys. Rev. Lett. 102: 011801
35. Rosner J L (2001) Charmless final states and S-D-wave mixing in the ψ'' . Phys. Rev. D 64: 094002, arXiv:0105327 [hep-ph]
36. Chao K T (2008) Interpretations for the X(4160) observed in the double charm production at B factories. Phys. Lett. B 661: 348-353, arXiv:0707.3982 [hep-ph]
37. Badalian A, Bakker B, Danilkin I (2009) The S-D mixing and di-electron widths of higher charmonium 1^{--} states. Phys. Atom. Nucl. 72: 638-646, arXiv:0805.2291 [hep-ph]
38. Choi S K, et al. (Belle Collaboration) (2003) Observation of a narrow charmonium-like state in exclusive $B^+ \rightarrow K^+ \pi^+ \pi^- J/\psi$ decays. Phys. Rev. Lett. 91: 262001, arXiv:0309032 [hep-ex]
39. CDF Collaboration (2007) Analysis of the Quantum Numbers J^{PC} of the X(3872) Particle. Phys. Rev. Lett. 98: 132002, arXiv:0612053 [hep-ex]
40. Aubert B, et al. (BABAR Collaboration) (2009) Evidence for $X(3872) \rightarrow \psi(2S)\gamma$ in $B^\pm \rightarrow X(3872) K^\pm$ decays, and a study of $B \rightarrow c\bar{c}\gamma K$. Phys. Rev. Lett. 102: 132001, arXiv:0809.0042 [hep-ex]
41. Abe K, et al. (Belle Collaboration) (2005) Evidence for $X(3872) \rightarrow \gamma J/\psi$ and the sub-threshold decay $X(3872) \rightarrow \omega J/\psi$. arXiv:0505037 [hep-ex]
42. del Amo Sanchez P, et al (BABAR Collaboration) (2010) Evidence for the decay $X(3872) \rightarrow J/\psi \omega$. Phys. Rev. D 82: 011101
43. Uehara S, et al. (Belle Collaboration) (2010) Observation of a charmonium-like enhancement in the $\gamma\gamma \rightarrow \omega J/\psi$ process. Phys. Rev. Lett. 104: 092001, arXiv: 0912.4451 [hep-ex]
44. Choi S K, et al. (Belle Collaboration) (2005) Observation of a near-threshold $\omega - J/\psi$ mass enhancement in exclusive $B \rightarrow K\omega J/\psi$ decays. Phys. Rev. Lett. 94: 182002, arXiv:0408126 [hep-ex]

-
45. Aubert B, et al. (BABAR Collaboration) (2008) Observation of $Y(3940) \rightarrow J/\psi\omega$ in $B \rightarrow J/\psi\omega K$ at BABAR. Phys. Rev. Lett. 101: 082001, arXiv:0711.2047 [hep-ex]
 46. Eichten E J, Lane K, Quigg C (2004) Charmonium levels near threshold and the narrow state $X(3872) \rightarrow \pi^+\pi^- J/\psi$. Phys. Rev. D 69: 094019
 47. Yang Y C, Xia Z R, Ping J L (2010) Are the $X(4160)$ and $X(3915)$ charmonium states? Phys. Rev. D 81: 094003
 48. Zhao Z J, Pan D M (2011) Estimating strong decays of $X(3915)$ and $X(4350)$. arXiv:1104.1838 [hep-ph]
 49. Yang Y C, Ping J L (2010) Dynamical study of the $X(3915)$ as a molecular $D^*\bar{D}^*$ state in a quark model. Phys. Rev. D 81: 114025, arXiv:1004.2444 [hep-ph]
 50. Bugg D V (2011) Explanation for $Y(4140)$ and $X(3915)$. arXiv:1103.5363 [hep-ph]
 51. Branz T, Gutsche T, Lyubovitskij V E (2009) Hadronic molecule structure of the $Y(3940)$ and $Y(4140)$. Phys. Rev. D 80: 054019, arXiv:0903.5424 [hep-ph]
 52. Abe K, et al. (Belle Collaboration) (2007) Observation of a new charmonium state in double charmonium production in e^+e^- annihilation at $\sqrt{s} \sim 10.6$ GeV. Phys. Rev. Lett. 98: 082001, arXiv:0507019 [hep-ex]
 53. Eichten E J, Lane K, Quigg C (2006) New states above charm threshold. Phys. Rev. D 73: 014014
 54. Uehara S, et al. (Belle Collaboration) (2006) Observation of a χ'_{c2} candidate in $\gamma\gamma \rightarrow D\bar{D}$ production at Belle. Phys. Rev. Lett. 96: 082003, arXiv:0512035 [hep-ex]
 55. Aubert B, et al. (BABAR Collaboration) (2010) Observation of the $\chi_{c2}(2P)$ meson in the reaction $\gamma\gamma \rightarrow D\bar{D}$ at BABAR. Phys. Rev. D 81: 092003, arXiv:1002.0281 [hep-ex]
 56. Barnes T (2010) Update on charmonium theory. arXiv:1003.2644 [hep-ph]
 57. Swanson E S (2006) The new heavy mesons: A status report. Phys. Rep. 429: 243-305
 58. Pakhlov P, et al. (Belle Collaboration) (2008) Search for new charmonium states in the processes $e^+e^- \rightarrow J/\psi D^* D^*$ at $\sqrt{s} \sim 10.6$ GeV. Phys. Rev. Lett. 100: 202001, arXiv:0708.3812 [hep-ex]
 59. Shen C P, et al. (Belle Collaboration) (2010) Evidence for a new resonance and search for the $Y(4140)$ in $\gamma\gamma \rightarrow \varphi J/\psi$. Phys. Rev. Lett. 104: 112004, arXiv:0912.2383 [hep-ex]
 60. Liu X, Luo Z G, Sun Z F (2010) $X(3915)$ and $X(4350)$ as new members in the P-wave charmonium family. Phys. Rev. Lett. 104: 122001
 61. Zhang J R, Huang M Q (2010) $\{Q\bar{s}\}\{\bar{Q}'s\}$ molecular states in QCD sum rules. Commun. Theor. Phys. 54: 1075-1090, arXiv:0905.4672 [hep-ph]
 62. Ma Y L (2010) Estimates for $X(4350)$ decays from the effective lagrangian approach. Phys. Rev. D 82: 015013, arXiv:1006.1276 [hep-ph]
 63. Stancu F (2010) Can $Y(4140)$ be a $c\bar{c}s\bar{s}$ tetraquark? J. Phys. G 37: 075017
 64. Wang Z G (2010) Analysis of the $X(4350)$ as a scalar $\bar{c}c$ and $D_s^*\bar{D}_s^*$ mixing state with QCD sum rules. Phys. Lett. B 690: 403, arXiv:0912.4626 [hep-ph]
 65. Dudek J J, Edwards R G, Thomas C E (2009) Exotic and excited-state radiative transitions in charmonium from lattice QCD. Phys. Rev. D 79: 094504
 66. Li G, Zhao Q (2011) Revisit the radiative decays of J/ψ and $\psi' \rightarrow \gamma\eta_c(\gamma\eta'_c)$. Phys. Rev. D 84: 074005, arXiv:1107.2037 [hep-ph]
 67. Chen H, Ping R G (2009) Charmonium rescattering effects in $\psi' \rightarrow \gamma\eta_c$ decay. Eur. Phys. J. A 42: 237